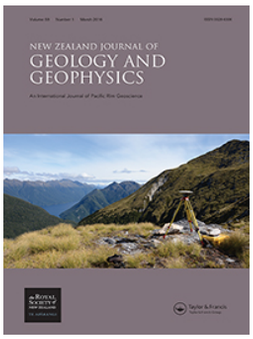

New Zealand Journal of Geology and Geophysics

ISSN: 0028-8306 (Print) 1175-8791 (Online) Journal homepage: https://www.tandfonline.com/loi/tnzg20

A geodetic study of Otago: results of the central Otago deformation network 2004–2014

P Denys, C Pearson, R Norris & M Denham

To cite this article: P Denys, C Pearson, R Norris & M Denham (2016) A geodetic study of Otago: results of the central Otago deformation network 2004–2014, New Zealand Journal of Geology and Geophysics, 59:1, 147-156, DOI: 10.1080/00288306.2015.1134592

To link to this article: https://doi.org/10.1080/00288306.2015.1134592

NEW ZEALAND JOURNAL OF GEOLOGY AND GEOPHYSICS, 2016
VOL. 59, NO. 1, 147–156
http://dx.doi.org/10.1080/00288306.2015.1134592

Taylor & Francis
Taylor & Francis Group

RESEARCH ARTICLE

A geodetic study of Otago: results of the central Otago deformation network 2004–2014

P Denys[a], C Pearson[a], R Norris[b] and M Denham[a]

[a]School of Surveying, University of Otago, Dunedin, New Zealand; [b]Department of Geology, University of Otago, Dunedin, New Zealand

ABSTRACT

We have analysed 11 years of geodetic data from 30 stations distributed over the Otago Fault System in the South Island of New Zealand. Velocities were estimated from time series corrected for coseismic displacements from the 2004 Macquarie Island and 2007 George Sound earthquakes and the coseismic and the short term postseismic deformation associated with the 2009 Dusky Sound earthquake. By dividing the corrected time series in half we were able to demonstrate the existence of a systematic difference between the pre- and post-earthquake velocity fields, associated with a longer term viscoelastic transient related to the 2009 Dusky Sound earthquake. In the northern part of our study area, the geodetic strain rate data are consistent with elastic strain accumulation on the Alpine Fault while in the south and east, the strain rate tensors are consistent with the Otago Fault System. There is a significant change in orientation in the axis of contraction from east to west across the network that correlates with a transition between the Otago and Waihemo Fault Systems. We also demonstrate significant spatial variation in the rates of strain accumulation that may correlate with active and quiescent parts of the Otago Fault System. However these strain rates represent the average values for the 11 years that the COD network has been observed and may also be influenced by the longer term viscoelastic transient related to the Dusky Sound earthquake.

ARTICLE HISTORY
Received 28 May 2015
Accepted 12 December 2015

KEYWORDS
Fault processes; geodetic strain; New Zealand active tectonics; plate boundary processes; tectonics

Introduction

Central Otago is located in the southern half of the South Island of New Zealand in an area of spectacular ridges and valleys that are thought to define a series of actively growing asymmetric anticlines above blind reverse faults (Jackson et al. 1996). These structures have been the subject of several studies that established that individual faults are periodically active followed by long periods of quiescence when the activity migrates to another structure in the region (Beanland & Berryman 1989; Litchfield & Norris 2000). Because of the episodic nature of the deformation it was not known which structures are active and which are not. Prior to this study, the area has not been the subject of detailed geodetic measurements since the advent of satellite geodesy advent of satellite geodesy, although a few studies have looked at deformation in the Otago region with a sparse GPS dataset (e.g. Beavan & Haines 2001; Beavan et al. 2007; Wallace et al. 2007). The studies that do exist from the 1980s (Blick 1986; Pearson 1990) are based on the analysis of triangulation measurements, which are subject to large errors. This study, which has used the Central Otago Deformation (COD) network, seeks to better define the contemporary deformation using modern satellite-based techniques. This paper updates preliminary results from Denys et al. (2014) (which used geodetic data through 2009) by incorporating an extra 6 years of data and nearly doubling the study area.

Central Otago deformation network

The COD network consists of a series of geodetic marks developed so that each site has easy, all weather access (two-wheeled drive vehicle) as well as a secure site so that the equipment could be left unattended for long periods of time. To overcome the centreing and antenna height error inherent in traditional GPS campaigns, each antenna is connected to a fixed height adaptor that is directly attached to a 5/8" threaded rod that is epoxied into rock. The height of the antenna reference point above the ground depends on the length of the fixed height adaptor and generally ranges between 0.055 m and 0.1 m. The COD network sites used in this analysis are shown as blue and black triangles (Figure 1) and the cGPS sites of the LINZ PositionNZ network, are shown as red triangles.

The first sequence of COD marks was established in 2004, a second phase established in late 2005 and a third phase in 2009. The mark distribution is governed by the layout of the road network, which in turn tends to follow the valleys and basins of the region. This allows for easy and fast access to the marks, but does result in the mark distribution being biased towards

CONTACT C Pearson chris.pearson@otago.ac.nz
Supplementary data available online at www.tandfonline.com http://dx.doi.org/10.1080/00288306.2015.1134592

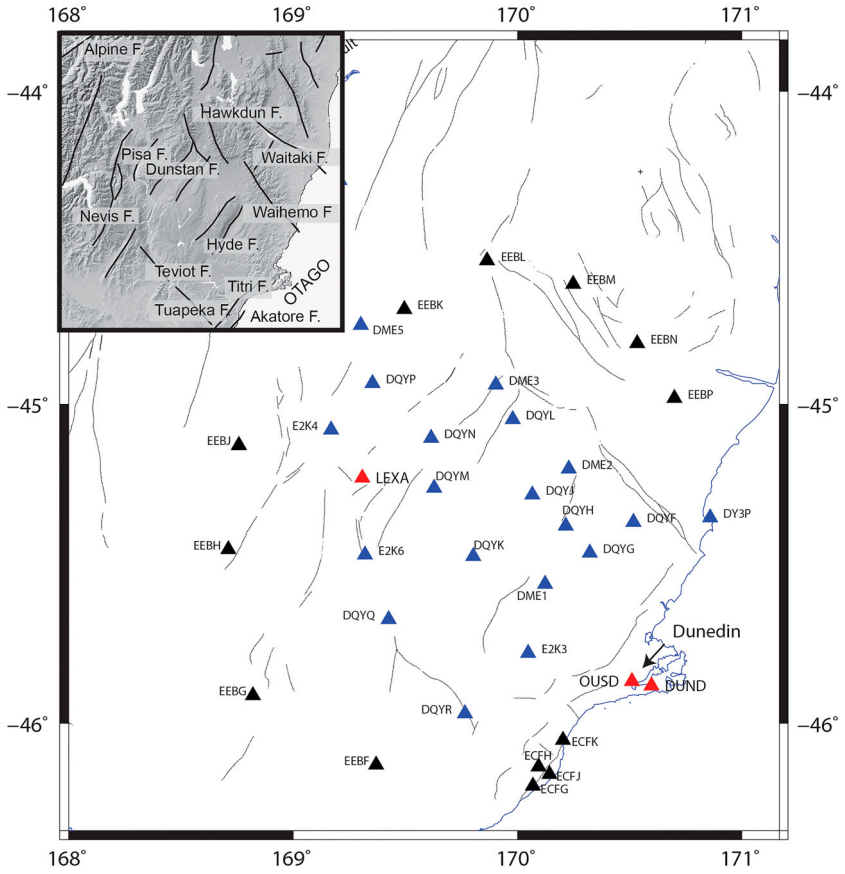

Figure 1. COD sites established in 2004–2005 (blue triangles), COD sites established in 2009 are shown as black triangles and LINZ PostioNZ sites (red triangles). The Waihemo Fault, Alpine Fault and Otago Fault System NE trending faults (after Upton et al. (2009)) are shown in inset.

lower elevations. The surveys have been conducted using a fairly consistent set of equipment. All of the measurements since 2004 have used Trimble 5700, R7 and R10 receivers and Trimble Geodetic, Trimble Geodetic 2 or R10 antennas. The GPS data were processed using standard double differencing techniques (Bernese v5.2) using the ITRF2008 reference frame (see Dataset S1 for a detailed discussion). The sites were initially occupied at least twice a year; after December 2012, this was reduced to a single annual occupation. Points are normally occupied for 4 days. Velocities were calculated from the position time series using Matlab scripts developed at the School of Surveying, University of Otago. Formal errors of GPS velocity estimates are well-known to be unrealistically small (Williams et al. 2004) so, following Beavan et al. (2016), we incorporated 1.1 mm/yr of white noise values and 1 mm/yr$^{1/2}$ of random walk noise to the east and north components of the velocity uncertainties.

Campaign GPS

Along with the COD network, the velocity field of the South Island is defined by the LINZ PositioNZ continuous GPS (cGPS) network, augmented by continuous stations operated by GeoNet (www.geonet.org.nz) and the University of Otago, and an extensive network of campaign measurements collected over the last 20 years by the University of Otago in collaboration with GNS Science under the leadership of John Beavan. The campaign network data has been collected using traditional GPS methods: tripod, tribrach and antenna with nominally 2-day (48 hr) observing sessions, although some of the earlier campaigns were observed with sessions of less than 24 hrs. While this method is versatile and expedient, it is prone to centring and antenna height measurement errors. The use of different equipment (e.g. antenna) between campaigns, can result in positional errors. This is particularly true for the early measurements in the 1990s when the antenna phase centre models were significantly less accurate than for more modern antennae. For these reasons we have not incorporated the non-COD campaign measurements in our study.

Correction for coseismic and postseismic deformation

Earthquakes since 2004 have produced substantial coseismic displacements over a large swath of the South Island and one of these, the ML 7.8 2009 Dusky Sound Earthquake has caused significant postseismic deformation. As a result, the GPS

measurements have to be corrected for this deformation before they can they can be used for velocity estimates. For the cGPS sites located in the study area (OUSD, DUND and LEXA), we were able to estimate both the coseismic and postseismic deformation from the times series. However for the COD marks, which were nominally surveyed at 6-month intervals, we found that there was insufficient data to simultaneously estimate these parameters so we had to use a modified procedure where the coseismic and postseismic deformation were interpolated from grid files and the velocity is then estimated from the corrected time series.

Corrections derived from the cGPS time series

The School of Surveying's Matlab script (PTS) has the capability of estimating both the coseismic and postseismic deformation from the position time series. The coseismic deformation is modelled as a Heaviside step function that is zero if $t < t_e$ (where t_e is the time of the earthquake and t is the time of measurement) and one for $t \geq t_e$. That is

$$\left.\begin{array}{ll} D_j(\phi, \lambda, t) = 0 & \\ D_j(\phi, \lambda, t) = \mathrm{C_j}(\phi, \lambda) & \end{array}\right\} \begin{array}{l} t < t_e \\ t \geq t_e \end{array} \quad (1)$$

where $C_j(\phi, \lambda)$ is the coseismic offset for event t_e with latitude ϕ and longitude λ and $D_j(\phi, \lambda, t)$ is the offset applied at time t. The dimension j represents the position component i.e. j = east, north, up.

The postseismic deformation is more complicated to model because it is the product of two main physical processes (after-slip and viscoelastic relaxation), that have approximately logarithmic and exponential decays with time. However, by examining the time series of cGPS stations affected by the 2009 Dusky Sound earthquake we find that a logarithmic decay function adequately fits all of the measured postseismic decay data. We made no effort to correct for postseismic deformation for any of the other Fiordland earthquakes because there was insufficient data available.

For the purposes of correcting the time series we use the logarithmic decay function to model the postseismic decay as:

$$\left.\begin{array}{l} P_j(\phi, \lambda, t) = 0 \\ P_j(\phi, \lambda, t) = A_j(\phi, \lambda)\left[1 + \log\left(\dfrac{t - t_e}{\tau}\right)\right] \end{array}\right\} \begin{array}{l} t < t_e \\ t \geq t_e \end{array} \quad (2)$$

Here $P_j(\phi, \lambda, t)$ represents the cumulative postseismic displacement from time t_e to time t, the amplitude $A_j(\phi, \lambda)$ is given for dimension j (east, north, up), latitude ϕ and longitude λ, t_e is the time of occurrence of the earthquake, and τ is the relaxation constant associated with the earthquake. Note that the amplitude varies only with latitude and longitude but not with time. The total deformation associated with an earthquake event is the sum of $D_j(\phi, \lambda, t)$ and $P_j(\phi, \lambda, t)$.

For the cGPS, the parameters $C_j(\phi, \lambda)$ from Equation (1) and $A_j(\phi, \lambda)$ from Equation (2) were estimated from the time series together with the velocity using a non-linear least squares procedure.

Correction applied to the COD time series

For the COD marks, the velocity estimation was a two-step process. First the time series was corrected for coseismic and postseismic displacements using parameters interpolated from grid files. Then the velocity was estimated using the least squares procedure coded into PTS.

The first step was to correct time series for the coseismic displacements for the three Fiordland earthquakes that occurred since the COD network was established and had a large enough displacement to significantly affect the time series (ML 8.1 2004 Macquarie Island, ML 6.7 2007 George Sound and ML 7.8 2009 Dusky Sound). We developed grid files of the coseismic offsets based on dislocation models from Beavan et al. (2010) (Datasets S1 and S2) for each event. We then estimated the coseismic by interpolating each grid file in turn and then corrected the time series using Equation (1). A similar procedure was used to develop the earthquake patches for the NZGD2000 deformation Model (Crook et al. 2016).

We used a similar procedure to correct the COD time series for postseismic deformation associated with the ML 7.8 2009 Dusky Sound Earthquake. As a first step we developed a grid file containing values of $A_j(\phi, \lambda)$. We used a uniform value of $\tau = 0.019$ yrs, based on non-linear least squares to estimation the decay time scale by stacking all the available cGPS position time series and estimating a common decay time scale but different coseismic displacements and decay amplitudes for each site. The short decay time that we estimate suggests that with this approach we will only be capturing short-term afterslip in our correction. The postseismic deformation grid was developed by gridding of the postseismic amplitude coefficients for 13 South Island cGPS stations (BALC, BLUF, DUND, HOKI, LEXA, MAVL, MTJO, OUS2, OUSD, PYGR, QUAR and WAIM) using the GMT gridding programme SURFACE. The grid extends from 40.75° S to 47° S in latitude and from 166.5° E to 172.75° E in longitude at a 0.25° grid spacing. We estimated the amplitude variable in Equations (1 and 2) ($A_j(\phi, \lambda)$ and $D_j(\phi, \lambda, t)$) from the grid files using linear interpolation techniques.

Once the postseismic amplitude coefficients are estimated, the contribution of postseismic deformation can be estimated for each observation epoch and then subtracted from the time series before the velocities were estimated. The effect of the postseismic

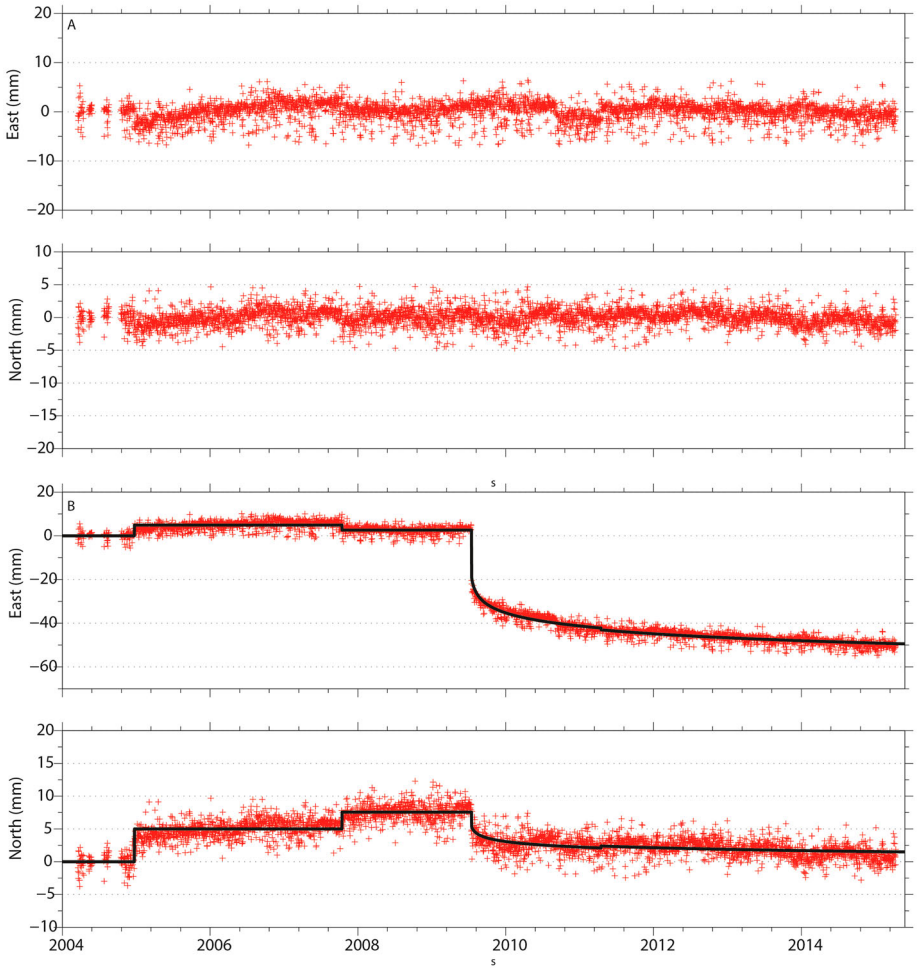

Figure 2. Modelled time series and residuals for station LEXA. Figure 2A shows the residuals derived using the postseismic deformation correction in Equation (2). Figure 2B shows the original time series. Red crosses represent daily coordinate estimates and the black line in Figure 2B represents the modelled time series.

deformation correction for LEXA is shown in Figure 2. Figure 2A shows the de-trended time series including the coseismic offset and the postseismic deformation while Figure 2B shows the residuals once the postseismic correction procedures described above have been applied.

In addition to the short term postseismic transient that we correct for, there are apparent longer term velocity changes at cGPS sites across the southern half of the South Island that probably represent a much longer term viscoelastic transient (with a long period time constant) related to the Dusky Sound earthquake. Since the time constant and amplitudes associated with the long term viscoelastic transient are not well understood at present, we have not corrected for these terms using the technique described above.

Cod velocity field

The site velocities shown in Figure 3 are in a Pacific Plate fixed reference frame using the Pacific Plate/ITRF2008 Euler pole from DeMets et al. (2014). We do not show velocities for DME2, which is on a known landslide. Figure 3A shows the velocities derived for the full data set, corrected for the postseismic deformation discussed in the previous section. Figure 3B uses only data recorded before July 2009 and therefore not affected by postseismic deformation correction and Figure 3C uses only data recorded after July 2009. Unfortunately only the subset of sites established in 2004–2005 (shown as blue triangles in Figure 1) have sufficient data for velocity determination using only pre-earthquake data. While the velocities shown in Figure 3B are noisier than those in Figure 3A, which is not surprising given the shorter data span available, the velocity fields are similar and do not suggest that the procedure we used to correct the site velocity determinations for postseismic deformation introduces bias. Over most of our study area, the velocity vectors have a generally northeast orientation with magnitudes increasing towards the Alpine Fault. The velocity vectors shown in Figure 3A–C are shown in Tables S1–S3.

In coastal Otago, particularly in the coast SW of Dunedin, the velocity vectors are heterogeneous with some indication of contraction between OUSD and DUND (which are moving towards each other at the sub-mm/yr level) while ECFG, ECFH, ECFJ and ECFK seem to diverge. Whether or not this

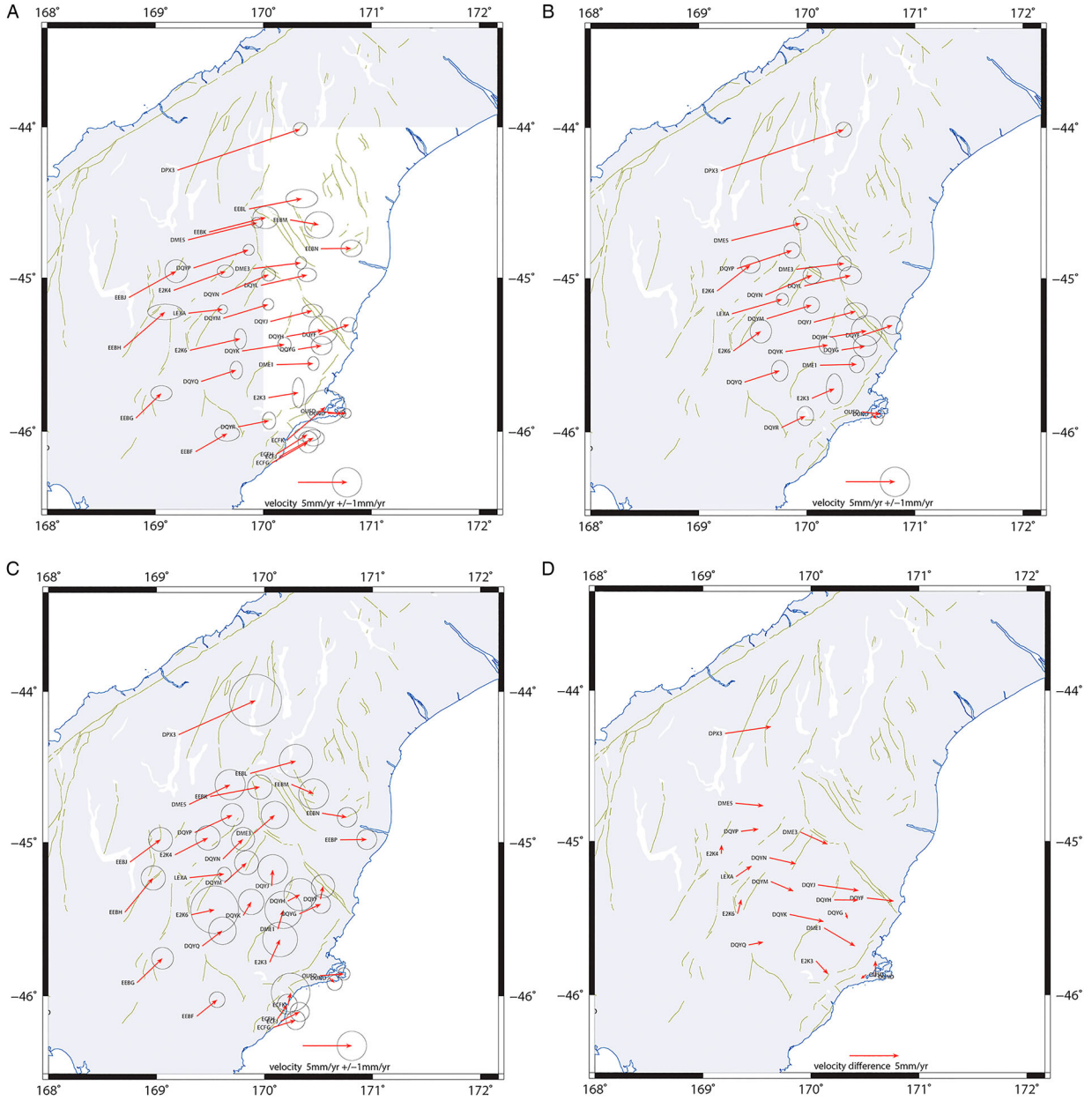

Figure 3. Velocity field rotated into a Pacific Plate fixed system. Error ellipses are at the 1-sigma level of confidence. Figure 3A shows velocities derived using the full data set. Figure 3B shows velocities derived using only data prior to the Dusky Sound 2009 -earthquake. Figure 3C shows velocity field derived using derived using only data after to the Dusky Sound 2009 earthquake. Figure 3D Difference between the velocities derived from the pre- and post-Dusky Sound earthquake data.

heterogeneity in deformation is real needs to be determined by future measurements at these sites.

Figure 3D shows the difference between the velocity measurements made using measurements before the Dusky Sound earthquake and those using data only from the post-earthquake period. The difference in velocity vectors show that there is a systematic difference between the two velocity fields. The difference seems to increase from east to west across the study area and indicates that the pre-earthquake velocity vectors have a larger easterly component and smaller northerly component than the post-earthquake velocities. This difference probably represents a velocity change associated with longer-term viscoelastic transient related to the Dusky Sound earthquake.

Another way to develop a velocity field that is not affected by the shorter term postseismic transient is to use only data recorded after this transient is negligible. In order to explore this option we estimated velocities using only occupations of the COD network recorded between 2011.0 and 2015.0. These velocities are discussed in Dataset S2. The main conclusion of our analysis is that the differences between the post-2011 velocities (shown in Figure S2) and the post-earthquake velocities with a short-term postseismic transient removed (shown in Figure 3C) is not significant at the 2-sigma level of confidence. This is shown in Figure S4 where we plot the differences between the post-2011 velocity vectors and the post-earthquake velocity vectors along with the combined error ellipses. The differential vectors

are small, randomly distributed and almost always plot within the 2-sigma error ellipses.

Strain rate analysis

We calculated the strain rate tensors for the five sub-networks (Figure 4A, Table 1) using the QOCA software (http://gipsy.jpl.nasa.gov/qoca). These calculations were done using velocities determined from all available data. Three Networks (A, C and E) yield strain rates between 20 and 50 ppb/yr, which are significantly larger than zero at the 95% level of confidence. In contrast, Networks B and W have rates of contraction of about 10 ppb/yr or less and are not significant at the 95% level of confidence. The strain rate tensors shown in Network A indicate predominantly shear strain while Networks E and C indicate predominantly contraction. Network E, which spans the NW trending Waihemo Fault System, has a strain tensor that is generally consistent with predominantly reverse motion on this fault. In contrast Network C's strain is not oriented perpendicular to the dominant NE trending structures as we would expect. The orientation of the principal axis of contraction for this network is poorly constrained, which may account for this apparent discrepancy. Generally our strain tensors are consistent with the single strain tensor for the Central Otago region shown by Beavan et al. (2007) Plate 1, in that the principal axis of contraction for most of our strain fall in the NW-SE quadrant like Beavan et al. (2007) and the tensors are consistent with shear strain (Network A) and contraction (Network C). The major exception to this is Network E where the orientation of the principal axis of contraction is in the NE-SW quadrant and the strain tensor is consistent with uniaxial contraction. The magnitudes of our maximum strain rates are variable. However, the three networks that have strain rates that are statistically different form zero have values about 40 ppb/yr which is quite similar to that of Beavan et al. (2007).

Table 1 Strain rates where the eigenvalue strain parameters, $\dot{\varepsilon}_{max}$ and $\dot{\varepsilon}_{min}$ are in the directions of the principle axes (eigenvectors). By convention, extension is positive with $\dot{\varepsilon}_{max} > \dot{\varepsilon}_{min}$. The angle θ is measured clockwise from north to the principal axis of the contraction. Errors are given at the 1-sigma level of confidence.

$\dot{\varepsilon}_{max}$	$\dot{\varepsilon}_{min}$	θ	Network
ppb/yr	ppb/yr	deg	
All data			
41 ± 6	−38 ± 7	114 ± 3	A
7 ± 7	−2 ± 8	349 ± 29	B
10 ± 9	−19 ± 8	95 ± 12	C
−6 ± 6	−46 ± 12	80 ± 9	E
8 ± 7	−5 ± 8	31 ± 22	W
Pre-Earthquake			
24 ± 7	−35 ± 9	108 ± 6	A
2 ± 9	−12 ± 11	94 ± 26	B
5 ± 9	−30 ± 12	110 ± 13	C
Post-Earthquake			
33 ± 13	−52 ± 18	101 ± 7	A
6 ± 13	−63 ± 15	109 ± 8	B
8 ± 24	−25 ± 17	36 ± 25	C
Post-Earthquake			
33 ± 13	−52 ± 18	101 ± 7	A
6 ± 13	−63 ± 15	109 ± 8	B
8 ± 24	−25 ± 17	36 ± 25	C
Beavan et al. (2016)			
40 ± 15	−36 ± 14	119 ± 8	A
30 ± 18	−21 ± 19	85 ± 15	B
0 ± 19	−10 ± 19	102 ± 84	C

The strain rate calculations depend on our procedure for correcting for postseismic deformation, which assumes that the velocities of the sites will be the same as before once the 0.019 yr decay time logarithmic transient is corrected for. However, as discussed above there is some evidence that the velocities may have indeed changed due to other, much longer lasting postseismic processes than the ones we are modelling. Consequently the strain rate tensors shown in Figure 4A represent the average values for the 11 years that the COD network has been running and do not necessarily represent the long term rate of elastic strain accumulation because of a possible longer term viscoelastic transient. In order to test the possibility that the strain rates have changed following the earthquake, we calculate the strain rate tensors for the three networks (Networks A, B and C) where all the stations have sufficient velocity data before the 2009 earthquake using only pre-earthquake data (Figure 4B) and only post-earthquake data (Figure 4C). The results of this calculation, (Table 1) do not differ significantly at the 95% level of confidence with the exception of Network B, which shows significantly more contraction for the post-earthquake data compared to the pre-earthquake data. The strain tensor for the post-earthquake data is consistent with contraction across the major thrust faults that dominate the tectonics in this area, instead of showing no significant strain accumulation as in the pre-earthquake data. This difference may indicate that velocity changes associated with a longer period viscoelastic transient related to the Dusky Sound earthquake have caused the rate of strain accumulation in Network B to increase significantly.

Beavan et al. (2016) tabulates the velocity vectors for a subset of the COD points. Since their velocity determination uses only pre Dusky Sound data, strain rates from their velocity field can be compared with our pre-earthquake results. The results (see Table 1) are nearly identical to our estimates for Network A and the other two agree within the 1-sigma level of confidence.

We expect the strain rate tensors from within the COD network to reflect the combined effects of the local Otago Fault System plus the influence of the Alpine Fault located to the northwest and slightly outside our area of study. We would expect Network A to have strain rate tensors consistent with a combination of reverse and dextral motion similar to the 055° trending Alpine Fault (Norris & Cooper 2001). The

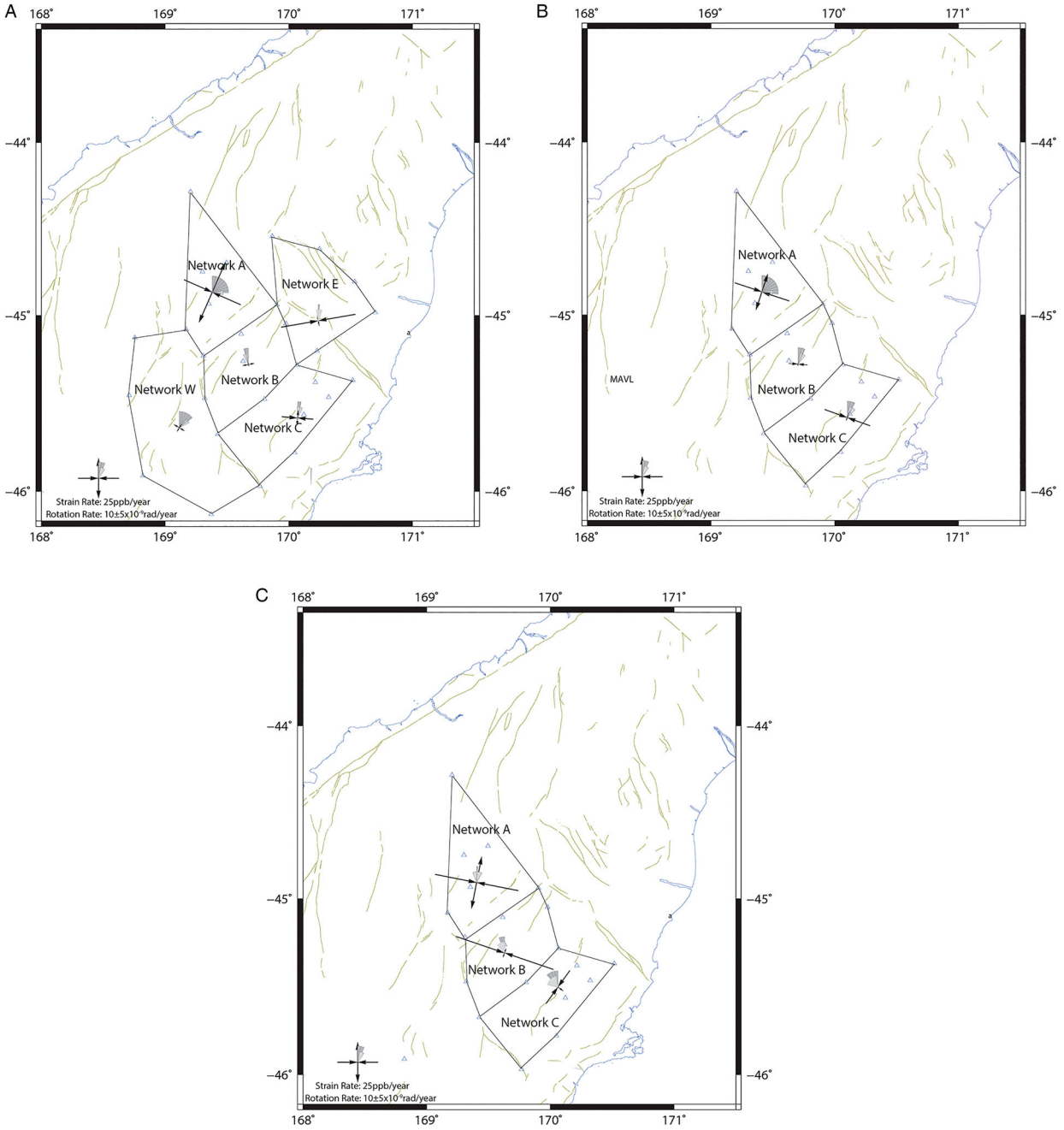

Figure 4. A, The strain networks and strain rates for the various sub-networks estimated from the velocity field in Figure 2. **B**, Strain rates calculated only from the pre-earthquake data. **C,** Strain rates calculated only from the post-earthquake data. Triangles indicate locations of velocity measurements used in strain determinations.

expectation is that the magnitude of the signature of the Alpine Fault should decrease as the distance from the Alpine Fault increases. Likewise the strain signature for the Otago Fault System should involve a negative dilatation and the principal axis of contraction should be more or less perpendicular to the average azimuth of the thrust faults. Since the average trend of these faults is about 020°, the principal axis of contraction would be expected to be oriented at about 110°. The southwestern and northeastern ends of the NE trending thrust faults that make up the Otago Fault System are terminated by a series of NW trending faults i.e. Teviot, Tuapeka and Waihemio (Craw et al. 2013; Curran et al. 2011; Upton et al. 2014). As a result, strain tensors for networks on the eastern and western edges of our study area that cross this transition might be expected to have strain tensors that are influenced by these features.

The strain rate shown in Network A is consistent with dextral shear (slightly transpressional) motion on the Alpine Fault. In Networks C and E the strain rate tensors are consistent with uniaxial contraction, which is what we would expect to be associated with local strain accumulation on the Otago Fault System. In Network C the principal axis of contraction is

oriented at an oblique angle to the azimuth of the NE trending thrust faults, however, the azimuth of the principal axis of contraction is poorly constrained. In contrast, Network E has strain tensor magnitudes significantly larger compared to Networks B and C. In the case of Network E the strain orientation of 081° ± 10°, which reflects the dominant influence of the NW trending Waihemo, Waitaki and Hawkdun Fault Systems. As discussed above the strain tensors from the full data set in Figure 4A have to be treated with caution due to the potential effect of a longer term viscoelastic transient related to the Dusky Sound earthquake. However, the strain rate tensors for the full data set and those derived only from the pre-earthquake data (Figure 4B) are similar so the results for Networks A. B and C are probably reasonably representative of the interseismic velocity field. Unfortunately there is insufficient pre-earthquake data to make the same comparison for Networks E and W.

We have five stations in coastal Otago (OUSD, ECFG, ECFH, ECFJ and ECFK), which are not incorporated into any strain network because the velocity vectors do not define a uniform strain field. The reason for these anomalous velocity vectors is not clear but it is noteworthy that they are all located close to the Akatore Fault. Because of the potential seismic hazard that this fault poses to Dunedin and other coastal communities in Otago this area should be a high priority for future geodetic measurements.

Discussion

The strain tensors shown in Figure 4A show a transition from predominantly shear strain in Network A to the north to predominantly contraction in Networks C and E. All other networks give results that are not significantly different from zero at the 95% level of confidence. The variation in strain rates is not unexpected given the evidence for periodic activity for faults in the Otago Fault System. Our results are consistent with the Waihemo Fault System currently being in an active phase, while the other members of the Otago Fault System are in a quiescent phase.

Velocity vectors in Coastal Otago are anomalous. In particular the vectors from OUSD and DUND seem to indicate contraction at the level of c. 1 mm/yr. The velocity field here is too heterogeneous to allow us to include it in our strain rate analysis but the anomalous velocity vectors seem to be spatially correlated with the Akatore Fault. Given the importance of this feature to the seismic risk of Dunedin we feel that further geodetic measurements should be made here.

There is evidence of variation in strain rate tensors along the strike of the plate boundary zone with the azimuth of the principal axis of contraction for Network E, in the NE side of our study area, being rotated about 30° clockwise relative to the Network A. Such a change of orientation is not unexpected given the change in the underlying tectonics from the central part of our study area, which is dominated by the NE trending structures of the Otago Fault System and Network E, which is dominated by the NW trending structures of the Waihemo Fault System. Upton et al. (2009) postulated a transition zone where the principal axis of compression is orientated parallel to the plate boundary in a broad corridor along the Waitaki River Valley in contrast to the surrounding parts of Otago and Canterbury where the principal axis of compression is orientated perpendicular to the plate boundary. The change in principal axis of contraction orientation between Network E on one hand, and Networks A on the other hand, is roughly coincident with the eastern edge of the transition zone of Upton et al. (2009).

Conclusions

We have analysed c. 11 years of recent satellite-based geodetic data from c. 30 stations distributed evenly over a broad corridor ex-tending from the north end of Lake Wanaka to Dunedin. Velocities were estimated from time series that were corrected for the coseismic displacements associated with the ML 8.1, 2004 Macquarie Island and ML 6.7 2007 George Sound earthquakes and the coseismic and postseismic deformation associated with the ML 7.8 2009 Dusky Sound earthquake. We divided the data into a series of sub-networks to study the variation of geodetic strain over the region.

The northern strain rate tensor (Network A) is consistent with dextral movement on the Alpine Fault and probably represents, at least in part, elastic strain accumulation on the Alpine Fault and other plate boundary structures outside our study area. The strain rate tensors in the reminder of the study area (Networks B, C, E and W) are consistent with uniaxial contraction as in Networks C and E or show no significant strain. There is a significant change in the orientation of principal axis of contraction between Network E, which overlies the Waihemo Fault System and Network A.

There is a significant change in the rate of strain accumulation over the various parts of the study area with some areas where the magnitude of the principal axis of contraction is about 40 ppb/yr and other areas where the rate of strain accumulation is not significantly different from zero. Given the evidence for periodic activity for faults in the Otago Fault System, we might expect that high rates of strain accumulation would be observed over faults that are in an active phase and low rates for faults that are not. Our results would suggest that the Waihemo Fault and possibly one of the faults located in Network C may be in an active phase now while

the others may be quiescent. There is some evidence that the region surrounding the Akatore Fault is characterised by high rates of contraction, but this is largely based on convergence between two cGPS stations in the Dunedin area, and requires further investigation. In order to develop more robust deformation rate estimates for this fault, we have established four new GPS sites in this region that will hopefully provide a more reliable estimate of the rate of strain accumulation associated with this fault in the future.

We have documented a significant change in the pre-earthquake and post-earthquake strain rate tensors for Network B. The strain tensor for the post-earthquake data is consistent with contraction across the major thrust faults that dominate the tectonics in this area instead of showing no significant strain accumulation as in the pre-earthquake data. This observation may be significant for Central Otago because the strain tensor is oriented such that the associated changes might be bringing the fault closer to failure. This demonstrates that that velocity changes associated with longer term viscoelastic transient related to the Dusky Sound earthquake needs to be carefully monitored.

Supplementary data

Dataset S1. Commentary on the GPS processing, including Tables S1–S3.

Table S1. Velocities derived for the full data set.

Table S2. Velocities derived for data set recorded before July 2009.

Table S3. Velocities derived from data recorded after July 2009.

Dataset S2. Analysis of the 2011.0 to present time series, including Table S4 and Figures S1–4.

Table S4. Strain rates where the eigenvalue strain parameters, $\dot{1}_{max}$ and $\dot{1}_{min}$ are in the directions of the principle axes (eigenvectors).

Figure S1. De-trended time series and residuals for station LEXA using post-2011 data only.

Figure S2. Velocity field derived from the post-2011 data rotated into a Pacific Plate fixed system using Altimimi.

Figure S3. The strain networks and strain rates for the various sub-networks estimated from the velocity field in Figure S2.

Figure S4. Differences between the post-2011 velocity vectors and the post-earthquake velocity vectors along with the combined error ellipses.

Acknowledgements

Fieldwork support undertaken by Alastair Neaves (School of Surveying) together with numerous University of Otago students. This manuscript benefited from a review by Phaedra Upton, Laura Wallace and one anonymous reviewer.

Guest Editor: Dr Laura Wallace.

Disclosure statement

No potential conflict of interest was reported by the authors.

Funding

This project has been funded by FRST through the GNS Science New Zealand Geological Hazards and Society Programme (C05X0804) with contributions to the Impacts of Global Plate Tectonics in and around New Zealand Programme (C05X02023). The initial establishment of this Central Otago deformation network was partly funded by an Earthquake Commission grant.

References

Beanland S, Berryman KR. 1989. Style and episodicity of late Quaternary activity on the Pisa-Grandview fault zone, central Otago, New Zealand. New Zeal J Geol Geophys. 32:451–461.

Beavan J, Ellis S, Wallace L, Denys P. 2007. Kinematic constraints from GPS on oblique convergence of the Pacific and Australian plates, central South Island, New Zealand. In: A continental plate boundary: tectonics at South Island, New Zealand. AGU Geophysical Monograph Series 175. Washington, DC: American Geophysical Union; p. 75–94.

Beavan J, Haines J. 2001. Contemporary horizontal velocity and strain-rate fields of the Pacific-Australian plate boundary zone through New Zealand. J Geophys Res. 106(B1):741–770.

Beavan J, Samsonov S, Denys P, Sutherland R, Palmer N, Denham M. 2010. Oblique slip on the Puysegur subduction interface in the 2009 July M_w 7.8 Dusky Sound earthquake from GPS and InSAR observations: implications for the tectonics of southwestern New Zealand. Geop J Int. 183:1265–1286.

Beavan RJ, Wallace LM, Palmer N, Denys P, Ellis S, Fournier N, Hreinsdottir S, Pearson C, Denham M. 2016. New Zealand GPS velocity field: 1995–2013. New Zeal J Geol Geophys. in press.

Blick GH. 1986. Geodetic determination of crustal strain from old survey data in Central Otago. In: Reilly WI, Harford BE, editors. Recent crustal movements of the Pacific region. Proceedings of the International Symposium. Wellington: Royal Society of New Zealand; p. 47–54.

Craw D, Upton P, Walcott R, Burridge C, Waters J. 2013. Tectonic controls on the evolution of the Clutha River catchment, New Zealand. New Zeal J Geol Geophys. 55:345–359.

Crook C, Donnelly N, Beavan J, Pearson C. 2016. From geophysics to geodetic datum: updating the NZGD2000 deformation model. New Zeal J Geol Geophys. doi:10.1080/00288306.2015.1128451.

Curran C, Norris R, Rieser U. 2011. The Waihemo Fault of north Otago: constraints on late Quaternary activity [Abstract]. In: Litchfield NJ, Clark K, editors. Geosciences 2011 Conference, Nelson, New Zealand: abstracts. Geoscience Society of New Zealand Miscellaneous Publication 130A: p. 29.

DeMets C, Marquez-Azua B, Cabral-Cano E. 2014. A new GPS velocity field for the Pacific Plate—part 1:

constraints on plate motion, intraplate deformation, and the viscosity of Pacific basin asthenosphere. Geophys J Int. 199:1878–1899.

Denys P, Norris R, Pearson C, Denham M. 2014. A geodetic study of the Otago Fault System of the South Island of New Zealand. In: Rizos C, Willis P, editors. Earth on the edge: science for a sustainable planet. Proceedings of the IAG General Assembly, Melbourne, Australia, June 28–July 2, 2011. International Association of Geodesy Symposia 139. Berlin: Springer-Verlag; p. 151–158.

Jackson J, Norris R, Youngson J. 1996. The structural evolution of active fault and fold systems in central Otago, New Zealand: evidence revealed by drainage patterns. J Struct Geol. 18:217–234.

Litchfield NJ, Norris RJ. 2000. Holocene motion on the Akatore Fault, South Otago coast, New Zealand. New Zeal J Geol Geophys. 43:405–418.

Norris RJ, Cooper AF. 2001. Late Quaternary slip rates and slip partitioning on the Alpine Fault, New Zealand. J Struct Geol. 23:507–520.

Norris RJ, Nicolls R. 2004. Strain accumulation and episodicity of fault movements in Otago. Earthquake Commission Research Report 01/445. Wellington: EQC Research Foundation.

Pearson C. 1990. Extent and tectonic significance of the Central Otago shear strain anomaly. New Zeal J Geol Geophys. 33:295–301.

Upton P, Craw D, Walcott R. 2014. Far-field deformation resulting from rheologic differences interacting with tectonic stresses: an example from the Pacific/Australian Plate boundary in Southern New Zealand. Geosciences. 4:93–113

Upton P, Koons PO, Craw D, Henderson CM, Enlow R. 2009. Along-strike differences in the Southern Alps of New Zealand: consequences of inherited variation in rheology. Tectonics. 28:TC2007. doi:10.1029/2008TC002353

Wallace LM, Beavan RJ, McCaffrey R, Berryman K, Denys P. 2007. Balancing the plate motion budget in the South Island, New Zealand using GPS, geological and seismological data. Geophys J Int. 168:332–352. doi:10.1111/j.1365-246X.2006.03183.

Williams SDP, Bock Y, Fang P, Jamason P, Nikolaidis RM, Prawirodirdjo L, Miller M, Johnson DJ. 2004. Error analysis of continuous GPS position time series. J Geophys Res. 109:B03412. doi:10.1029/2003JB002741.